Packet Size Optimization in Wireless Sensor Networks for Smart Grid Applications

Sinan Kurt, Huseyin Ugur Yildiz, *Member, IEEE*, Melike Yigit, Bulent Tavli, *Member, IEEE*, and Vehbi Cagri Gungor

***Abstract*—Wireless sensor networks (WSNs) are envisioned to be an important enabling technology for smart grid (SG) due to the low cost, ease of deployment, and versatility of WSNs. Limited battery energy is the tightest resource constraint on WSNs. Transmission power control and data packet size optimization are powerful mechanisms for prolonging network lifetime and improving energy efficiency. Increasing transmission power will reduce the bit error rate (BER) on some links, however, utilizing the highest power level will lead to inefficient use of battery energy because on links with low path loss achieving low BER is possible without the need to use the highest power level. Utilizing a large packet size is beneficial for increasing the payload-to-overhead ratio, yet, lower packet sizes have the advantage of lower packet error rate. Furthermore, transmission power level assignment and packet size selection are interrelated. Therefore, joint optimization of transmission power level and packet size is of utmost importance in WSN lifetime maximization. In this study, we construct a detailed link layer model by employing the characteristics of Tmote Sky WSN nodes and channel characteristics based on actual measurements of SG path loss for various environments. A novel mixed integer programming framework is created by using the aforementioned link layer model for WSN lifetime maximization by joint optimization of transmission power level and data packet size. We analyzed the WSN performance by systematic exploration of the parameter space for various SG environments through the numerical solutions of the optimization model.**

***Index Terms*—Mixed integer programming (MIP), network lifetime, packet size optimization, smart grid, transmission power control, wireless sensor networks.**

Manuscript received March 7, 2016; revised June 14, 2016 and August 15, 2016; accepted September 14, 2016. Date of publication October 21, 2016; date of current version February 9, 2017. The work of V. C. Gungor was supported by the Turkish National Academy of Sciences Distinguished Young Scientist Award Program (TUBA-GEBIP) under Grant V.G./TBA-GEBP/2013-14.

S. Kurt and B. Tavli are with the Department of Electrical and Electronics Engineering, TOBB University of Economics and Technology, Ankara 06520, Turkey (e-mail: skurt@etu.edu.tr; btavli@etu.edu.tr).

H. U. Yildiz is with the Department of Electrical and Electronics Engineering, TED University, Ankara 06420, Turkey (e-mail: hugur.yildiz@tedu.edu.tr).

M. Yigit is with the Department of Computer Engineering, Bahcesehir University, Istanbul 34353, Turkey (e-mail: melike.yigit@stu.bahcesehir.edu.tr).

V. C. Gungor is with the Department of Computer Engineering, Abdullah Gul University, Kayseri 38039, Turkey (e-mail: cagri.gungor@agu.edu.tr).

Color versions of one or more of the figures in this paper are available online at http://ieeexplore.ieee.org.

Digital Object Identifier 10.1109/TIE.2016.2619319

I. Introduction

SMART grid (SG) is a global networked cyber-physical system which is designed to efficiently orchestrate the global electric energy flow in the main electric arteries as well as in the single households [1], [2]. Wireless sensor networks (WSNs) are among the important constituents of SG [3], [4]. Indeed, sensing, monitoring, communications, and networking capabilities possessed by WSNs are highly desirable in various SG applications [5]. For example, WSNs can be deployed over various parts of the electric power grid (e.g., generation plants, power lines, renewable energy sites, etc.) [4]. Data related to the power usage, generation efficiency, and many other types of information can be measured, collected, and conveyed to a sink node (i.e., base station, operation center) for system and energy management issues [6]. Furthermore, perimeter security and physical intruder detection in SG facilities are also the potential application areas of WSNs [7]. One particular challenge in the utilization of WSNs in SG applications is the unique characteristics of SG environments which, typically, have harsh channel conditions [8]. In fact, the performance of WSNs is affected by channel characteristics, significantly [9].

Network lifetime is, arguably, the most important performance metric in WSNs. Since WSN nodes are battery operated, in general, optimal utilization of the limited battery energy is vital for prolonging the network lifetime. Energy budget of WSNs is dominated by the energy dissipation on communication [10]. Thus, optimization of all aspects of WSN communication and networking is the overarching goal. Adjusting the sensor nodes' duty cycle to facilitate the deep sleep mode for energy conservation is shown to be one of the important mechanisms for prolonging WSN lifetime. Avoiding redundant data transmissions by careful selection of data packet transmission frequency is, yet, another important mechanism for energy saving. Nevertheless, in this study, we focus on the optimization of two mechanisms, namely transmission power level and packet size, which can be utilized to mitigate the unnecessary energy dissipation in WSNs. Especially WSNs used in SG environments experience harsher channel conditions than most terrestrial WSN deployments [11], where packet size and transmission power optimization is imperative. While optimizing the packet size and transmission power, optimization of sensor nodes' duty cycle and transmission frequency should not be overlooked.

Optimization of packet size in WSNs is a topic extensively investigated in the literature. However, almost all studies on WSN packet size optimization are focused on specific

deployment environments other than SG environments (e.g., terrestrial WSNs [12]–[20], underwater WSNs [21]–[24], underground WSNs [25], and body area WSNs [26]–[28]). One exception is [29] which is the closest study to ours. In [29], the reliability of low power wireless links for various SG environments are investigated through simulations.

In this study, we systematically investigate the impact of conjoint optimization of data packet size and transmission power level on WSN lifetime in various SG environments. We built a link layer model based on the characteristics of Tmote Sky WSN platforms [30] and empirical SG path loss models [29]. The link layer model includes a rich set of energy dissipation terms and mechanisms which enables us to investigate WSN energy dissipation in detail. We built a mixed integer programming (MIP) framework on top of the link layer model for the analysis of WSNs deployed over SG environments. We explore the optimal transmission level and packet size characteristics for maximizing WSN lifetime in SG environments via the numerical solutions of the optimization model.

The main original contributions of our study are listed as follows.

1) A novel link layer model based on the Tmote Sky platform and SG path loss characteristics is built. This model enables us to perform analysis for the whole link layer handshake cycle (Acknowledgment—ACK—packets are transmitted to confirm the successful reception of data packets) which is ignored in all studies on WSN packet size optimization (i.e., either the existence of ACK packets or nonzero probability of failure for ACK packets are assumed).
2) A novel MIP framework is constructed which enables us to optimize the data packet size and transmission power level, jointly. In the literature, either the transmission power level is optimized by keeping the packet size constant or the packet size is optimized while keeping the transmission power level constant.
3) A large parameter space is systematically explored through the numerical solutions of the optimization model to characterize the extent of WSN lifetime maximization in SG environments by optimizing the packet size and transmission power level which has never been done in the literature.

The rest of the paper is organized as follows. The system model (i.e., link layer model and MIP framework) is elaborated in Section II. Numerical analysis is given in Section III. We present the conclusions of this study in Section IV.

II. System Model

In this study, we are not presenting the details of a novel communication protocol for maximizing SG WSN lifetime through data packet size optimization. Instead, we analyze the impact of packet size optimization in WSNs employed in SG environments within a general framework from the perspective of network lifetime maximization. Indeed, we do not dive into the details of specific MAC (medium access control)/routing algorithms or protocols. In fact, we utilize the MIP-based optimization of data flows for maximizing the network lifetime as an abstraction of an idealized cross-layer WSN protocol which encompasses the whole protocol stack. The most important advantage of such an abstraction is the elimination of the possible suboptimal behaviors of actual protocol implementation details that are not central to the optimization of packet size and transmission power in SG WSNs, *per se*.

In our framework, data flows, time division multiple access (TDMA) time slots allocations, and data packet sizes are optimized in a centralized manner by the base station. For a typical WSN, sufficiently long time elapses between network reorganization periods [31] (i.e., in all the scenarios, the left-hand side of (17) is at least an order of magnitude lower than the right-hand side), therefore, energy dissipation of route discovery and maintenance operations are only a small percentage (e.g., less than 1.0% [31]) of the total energy budget. Therefore, energy overhead for network maintenance can be ignored without resulting in a significant underestimation of total energy budget.

A conflict-free communication arrangement is obtained by employing a TDMA-based MAC layer which utilizes a timeslot assignment algorithm to mitigate interference among active links. Interference can be modeled by using a combinatorial interference model and by utilizing a conflict graph the scheduling constraints can be incorporated into the model. It is shown in [32] that such an algorithm is possible, hence, collision-free communication is achieved if sufficient bandwidth requirements are satisfied. In fact, in our model, we use the sufficient condition presented in [32] (i.e., (17) and (18)). Furthermore, it is reported in the literature that reduction of packet collisions to insignificant levels is possible by employing a dynamic TDMA approach in low overhead MAC protocols (e.g., DMAC is a time schedule-based MAC protocol designed to facilitate energy efficient data collection in WSNs [33]). Moreover, to avoid overhearing, adopting a TDMA-based channel access scheme is necessary.

A stationary WSN with multiple sensor nodes and a base station is considered for the SG application. Data packets generated at sensor nodes are transferred to the base station possibly via multihop paths. A TDMA mechanism is assumed to be in effect as elaborated in the proceeding paragraphs. Temporal dimension is arranged into equal duration rounds (T_{rnd}). In each round, each sensor node generates a certain amount of data packets (s_i). Details of the link layer are presented in Section II-A. Network lifetime optimization problem is outlined in Section II-B.

A. Link Layer Model

Our link layer is based on the characteristics of Tmote Sky motes, which are one of the widely utilized platforms for experimental WSN research, in general, and for WSN deployments at SG environments, in particular [3], [29]. Tmote Sky motes consist of Texas Instruments MSP430 microcontroller and Chipcon CC2420 radio. Eight transmission power levels and corresponding power consumptions are documented for Tmote Sky motes [30] and presented in Table I. Power consumption of Tmote Sky receiver for data reception is 69 mW (i.e., $P_{rx}^{\text{crc}} = 23$ mA $\times$ 3 V $= 69$ mW). Data acquisition energy is dissipated at each round on every node which is denoted as $E_{DA} = 57$ μJ. The power

TABLE I
TRANSMISSION POWER CONSUMPTION ($P_{tx}^{\text{CRC}}(l)$ IN MW) AND OUTPUT ANTENNA POWER ($P_{tx}^{\text{ant}}(l)$ IN DBM) AT EACH POWER LEVEL (l) FOR THE TMOTE SKY MOTES EQUIPPED WITH CC2420 FOR DIFFERENT POWER LEVELS (l) [30]

l	$P_{tx}^{\text{crc}}(l)$	$P_{tx}^{\text{ant}}(l)$	l	$P_{tx}^{\text{crc}}(l)$	$P_{tx}^{\text{ant}}(l)$
3 ($l_{\min}$)	25.5	−25	19	41.7	−5
7	29.7	−15	23	45.6	−3
11	33.6	−10	27	49.5	−1
15	37.5	−7	31 ($l_{\max}$)	52.2	0

consumption for data acquisition is obtained by adding the power for running the processor (5.4 mW) and the sensor board (6 mW) in active mode [30], [34] (i.e., $P_{DA} = 11.4$ mW). By multiplying P_{DA} with the total data acquisition and processing time ($T_{DA} = 5$ ms), E_{DA} is obtained. At each round all sensor nodes create a predetermined amount of data to be conveyed to the base station (e.g., at each $T_{\text{rnd}} = 40$ s round 120 Bytes of data is created by each sensor node). The payload size of a data packet is denoted by M_{PL} and assumed to take values of 120, 60, 40, 30, 24, and 20 Bytes. The number of data packets to be generated at each round by each sensor node depends on the payload size chosen. For example, only one data packet is generated by each sensor node if the payload size is chosen as 120 Bytes. However, if a payload size of 60 Bytes is chosen, then two data packets are generated at each round by each sensor node. As such, for each payload size chosen, the number of packets is adjusted so that the total amount of data generated at each round by each sensor node is fixed to 120 Bytes. The size of a data packet (M_P) including an 8-Byte header ($M_H = 8$ Bytes) varies between 28 and 128 Bytes, i.e., $M_P = M_{PL} + M_H$. ACK packet length is $M_A = 12$ Bytes.

There are predetermined time slots for data transmission between any pair of nodes. Time slots are cushioned by guard times from both ends to prevent synchronization errors [35], where the guard time is chosen to be $T_{\text{grd}} = 100$ μs, which is roughly twice the maximum synchronization error. The time interval from the instance that the data packet transmission completed to the instance that the ACK packet reception begins is composed of various delay constituents (e.g., propagation delay) and is modeled by T_{rsp} (100 μs). Data and ACK packet durations are denoted by $T_{tx}(M_P)$ and $T_{tx}(M_A)$, respectively, which are obtained by dividing the number of bits to the channel data rate ($\xi = 250$ Kbps). The slot time, which accounts for all of the aforementioned terms, can be expressed as $T_{\text{slot}} = [2 \times T_{\text{grd}} + T_{tx}(M_P) + T_{\text{rsp}} + T_{tx}(M_A)] = 4.78$ ms for $M_P = 128$ Bytes and $M_A = 12$ Bytes.

In the literature, there are many path loss models (analytical or experimental) proposed for WSNs [36], however, for accurate performance analysis, the model to be used must be customized for the specific site (i.e., through curve fitting the experimental data) [9]. Hence, we utilize the path loss models presented in [3], [29]. The models are given for both line-of-sight (LOS) and non-line-of-sight (NLOS) cases in the different SG environments (i.e., outdoor 500 kV substation, underground network transformer vault, and indoor main power control room at Georgia Power, Atlanta, GA, USA).

TABLE II
PATH LOSS MODEL PARAMETERS FOR VARIOUS SG ENVIRONMENTS [3]

Environment	Abbreviation	n	X_σ (dB)	P_n (dBm)
Outdoor 500 KV Substation (LOS)	OUS-L	2.42	3.12	−93
Outdoor 500 KV Substation (NLOS)	OUS-N	3.51	2.95	−93
Underground Network Transformer Vault (LOS)	UNT-L	1.45	2.45	−92
Underground Network Transformer Vault (NLOS)	UNT-N	3.15	3.19	−92
Indoor Main Power Room (LOS)	IMP-L	1.64	3.29	−88
Indoor Main Power Room (NLOS)	IMP-N	2.38	2.25	−88

The path loss on link-(i, j), Υ_{ij}, is given as

$$\Upsilon_{ij}[\text{dB}] = \Upsilon_0[\text{dB}] + 10n\log_{10}(d_{ij}/d_0) + X_\sigma \ \ [\text{dB}] \quad (1)$$

where d_{ij} is the distance between the transmitter and receiver, d_0 is a reference distance, Υ_0 is the path loss at the reference distance, n is the path loss exponent, and X_σ is a zero mean Gaussian random variable with the standard deviation σ in dB.

The received signal power due to a transmission at power level-l over the link-(i, j) is denoted as $P_{rx,ij}^{\text{ant}}(l)$ and obtained by

$$P_{rx,ij}^{\text{ant}}(l)[\text{dBm}] = P_{tx}^{\text{ant}}(l)[\text{dBm}] - \Upsilon_{ij}[\text{dB}]. \quad (2)$$

Since the transmission power level (l) is chosen on a link and path loss can be calculated from (1), the received power can be obtained by (2). Hence, SNR ($\psi_{ij}(l)$) is calculated as

$$\psi_{ij}(l)[\text{dB}] = P_{rx,ij}^{\text{ant}}(l)[\text{dBm}] - P_n[\text{dBm}] \quad (3)$$

where P_n is the noise power which includes the effect of total noise power on the effective receiver bandwidth and noise figure. Path loss parameters for the six SG measurement settings are presented in Table II.

In Tmote Sky motes, O-QPSK (offset-quadrature phase-shift keying) modulation is used. Bit error rate (BER) for O-QPSK is given by [37] as $p_e = Q(\sqrt{\frac{2E_b}{N_0}})$, where $\frac{E_b}{N_0} = \psi_{ij}(l)G_P$. In this notation, G_P is the process gain, that is, 8 for CC2420 radios ($\frac{2M\,\text{chip/s}}{250K\,\text{bit/s}}$) [38].

Hence, the probability of a successful packet reception of a φ-Byte packet transmitted at the power level-l over the link-(i, j) is

$$p_{ij}^s(l, \varphi) = \left(1 - Q\left(\sqrt{16\psi_{ij}(l)}\right)\right)^{8\varphi} \quad (4)$$

and failure probability is

$$p_{ij}^f(l, \varphi) = 1 - p_{ij}^s(l, \varphi). \quad (5)$$

A successful handshake occurs over the link-(i, j) when a data packet is transmitted at the power level-l by node-i and replied with an ACK packet transmitted at the power level-l by node-j (both packet receptions by the intended recipients should be successful). The probability of such an occurrence is

given as

$$p_{ij}^{HS,s}(l,k) = p_{ij}^{s}(l,M_P) \times p_{ji}^{s}(k,M_A). \quad (6)$$

Therefore, the probability of a failed handshake is expressed as

$$p_{ij}^{HS,f}(l,k) = 1 - p_{ij}^{HS,s}(l,k). \quad (7)$$

On the average, data packets have to be transmitted $\lambda_{ij}(l,k) = \frac{1}{p_{ij}^{HS,s}(l,k)}$ times. Energy dissipation for transmitting an M_P-Byte packet from node-i to node-j at power level-l is

$$E_{tx}^{D}(l,M_P) = P_{tx}^{\text{crc}}(l)T_{tx}(M_P). \quad (8)$$

During a time slot, a node is in the receive mode after the packet transmission is completed. Therefore, the total energy dissipation is the sum of transmit energy during transmission $T_{tx}(M_P)$ and receive energy during rest of the slot $T_{\text{slot}} - T_{tx}(M_P)$, which can be expressed as

$$E_{tx}^{HS}(l,M_P) = E_{tx}^{D}(l,M_P) + P_{rx}^{\text{crc}}(T_{\text{slot}} - T_{tx}(M_P)). \quad (9)$$

The energy dissipation for packet processing and transmitter including all retransmissions due to packet failures can be expressed as

$$E_{tx,ij}^{D}(l,k) = E_{PP} + \lambda_{ij}(l,k)E_{tx}^{HS}(l,M_P) \quad (10)$$

where E_{PP} is the one-time energy dissipation for packet processing. Therefore, for all retransmissions, there would be no additional processing energy consumed. To obtain the energy dissipation for packet processing (E_{PP}), power consumption of the platform (Tmote Sky mote) in active state (5.4 mW) [30] and per packet processing time should be multiplied (e.g., $E_{PP} = 12.66$ μJ for $M_{PL} = 120$ Bytes).

Energy dissipation for receiving a data packet and replying with an ACK packet can be expressed as

$$E_{rx}^{HS,s}(k,M_A) = P_{rx}^{\text{crc}}(T_{\text{slot}} - T_{tx}(M_A)) + E_{tx}^{A}(k,M_A). \quad (11)$$

If the handshake failure is due to the ACK packet reception, then energy dissipation on the receiver side is not affected. If the handshake failure occurs at the data packet reception path, then at the receiver side the energy cost will be

$$E_{rx}^{HS,f} = P_{rx}^{\text{crc}}T_{\text{slot}}. \quad (12)$$

Energy dissipation on the receiver side including all retransmissions is given as

$$\begin{aligned} E_{rx,ji}^{D}(l,k) = \; & E_{PP} + \lambda_{ij}(l,k)\Big[p_{ij}^{HS,s}(l,k)E_{rx}^{HS,s}(k,M_A) \\ & + p_{ij}^{s}(l,M_P)p_{ji}^{f}(k,M_A)E_{rx}^{HS,s}(k,M_A) \\ & + p_{ij}^{f}(l,M_P)E_{rx}^{HS,f}\Big]. \end{aligned} \quad (13)$$

B. MIP Framework

The MIP framework presented in this section is designed to maximize the WSN lifetime by utilizing the link layer model constructed in Section II-A. The network is represented as a directed graph (i.e., $G = (V, A)$), where V represents the set of all sensor nodes. By denoting node-1 as the base station, we define the set W to represent all nodes excluding the base station (i.e., $W = V \setminus \{1\}$). $A = \{(i,j) : i \in W, j \in V - i\}$ is the set of arcs. The *integer* valued f_{ij} represents the amount of data packets transmitted by node-i and received by node-j. The objective function and constraints of our model are presented in Fig. 1. Note that the objective in our framework is the maximization of the network lifetime in terms of seconds, which can be expressed by the product $N_{\text{rnd}} \times T_{\text{rnd}}$, where the variable N_{rnd} represents the lifetime of the network in terms of cumulative number of rounds.

The *flow balance* constraint is given in (14). It simply states that at every node-i, generated data is equal to the difference between the outgoing data flow and incoming data flow. Equation (15) represents the *total busy time* for each sensor node which is the sum of data acquisition time, packet receive time, and packet transmit time including the retransmissions. If a node is not busy during a time slot, then it is in sleep mode. Sleep mode power consumption is used as 3 μW (i.e., $P_{\text{slp}} = 3$ μW). *Energy constraint* at each node is represented by (16) and the left-hand side of this constraint is the sum of transmission, sleep, reception, and acquisition energies. The right-hand side of this constraint is the energy of batteries in sensor nodes ($\varrho =$ 15 KJ for each node). Equation (17) states that the *channel bandwidth* required for communications at each node cannot exceed the available bandwidth. The cumulative time spent on data reception (incoming flows), data transmission (outgoing flows), and blocked time (interfering flows) for all nodes cannot be larger than the total network lifetime. This constraint is adopted from the sufficient condition presented in [39]. Interfering flows are the flows around node-i which are not flowing into or flowing out of node-i, however, affect the available bandwidth of node-i. Interference function ($I_{jn}^{i}(l,k)$) is formulated in (18). If node-i is in the interference region of the transmission from node-j to node-n at power level-l (data transmission) or node-n to node-j at power level-k (ACK transmission), then the value of interference function for node-i is unity ($i \neq j \neq n$), otherwise it is zero. Equation (19) states that all flows are *nonnegative*.

The MIP model presented in Fig. 1 assumes a link-level transmission power control mechanism, where the power levels for both data and ACK packets are optimized on each link by considering the energy dissipations on each link (given in (10) and (13)). We assume that on link-(i,j), data packets are transmitted at power level-l_{ij}^{opt} by node-i, and ACK packets are transmitted at power level-k_{ji}^{opt} by node-j. These optimal power levels are determined by using the following link scope optimization scheme [10]:

$$\{l_{ij}^{\text{opt}}, k_{ji}^{\text{opt}}\} = \underset{l \in S_L \, k \in S_L}{\arg\min} \left(E_{tx,ij}^{D}(l,k) + E_{rx,ji}^{D}(l,k) \right). \quad (14)$$

It is shown in [40] that the maximum lifetime problem in WSNs with convergecast traffic (i.e., all traffic terminates at the base station) and integral flows (i.e., the flow variables are integers) is NP-complete if there are multiple topologies for the convergecast (i.e., multiple topology convergecast). In this context, single topology convergecast means that each generated data packet of each sensor node is delivered to the base station by using exactly the same path at each round. If multiple

Maximize N_{rnd}

Subject to:

$$\sum_{(i,j)\in A} f_{ij} - \sum_{(j,i)\in A} f_{ji} = N_{rnd} s_i \ \forall i \in W \tag{15}$$

$$T_{bsy,i} = T_{slot}\left[\sum_{(i,j)\in A} \lambda_{ij}(l,k) f_{ij} + \sum_{(j,i)\in A} \lambda_{ji}(l,k) f_{ji}\right] + N_{rnd} T_{DA}, \forall i \in W \tag{16}$$

$$\underbrace{\sum_{(i,j)\in A} E^{D}_{tx,ij}(l,k) f_{ij}}_{\text{transmission}} + \underbrace{P_{slp}(N_{rnd}T_{rnd} - T_{bsy,i})}_{\text{sleep}} + \underbrace{\sum_{(j,i)\in A} E^{D}_{rx,ji}(l,k) f_{ji}}_{\text{reception}} + \underbrace{N_{rnd}E_{DA}}_{\text{acquisiton}} \leq \varrho \ \forall i \in W \tag{17}$$

$$T_{slot}\left[\sum_{(i,j)\in A} \lambda_{ij}(l,k) f_{ij} + \sum_{(j,i)\in A} \lambda_{ji}(l,k) f_{ji} + \sum_{(j,n)\in A} \lambda_{jn}(l,k) f_{jn} I^{i}_{jn}(l,k)\right] \leq N_{rnd} T_{rnd}, \ \forall i \in V \tag{18}$$

$$I^{i}_{jn}(l,k) = \begin{cases} 1 \text{ if } P^{ant}_{rx,ji}(l) \geq P_{sns} \text{ or } P^{ant}_{rx,ni}(k) \geq P_{sns} \\ 0 \text{ o.w.} \end{cases} \tag{19}$$

$$f_{ij} \geq 0 \ \forall (i,j) \in A \tag{20}$$

Fig. 1. Mixed integer programming (MIP) framework.

paths are used for data packet delivery at different rounds, then the problem is a multiple topology convergecast. Since the MIP problem given in Fig. 1 is a multiple topology convergecast problem with integral flows for network lifetime maximization, it is an NP-complete problem.

In comparison to the existing body of work on packet size optimization in WSN literature [12], [15], [29], our approach differs in several ways. Studies on simulation-based analysis of packet size optimization (e.g., [29]) utilize various heuristic approaches which are not guaranteed to determine the optimal operation conditions, therefore, the results of those studies do not necessarily give the optimal solutions. However, in our approach, we present the results of optimal solutions. On the other hand, studies on mathematical modeling of packet size optimization (*e.g.*, [15]) use rather simplistic abstractions to facilitate the tractability of the models, therefore, the impact of many important mechanisms are ignored in such models. However, in our framework, we incorporated a very rich set of mathematical abstractions of actual platforms and propagation environments.

Iterative optimization is an approach utilized in many studies on WSNs (e.g., performance optimization in real-time operation of fault-tolerant control systems) [4]. To apply iterative optimization, the problem should have a structure that enables convergence to the optimal solution by successive iterations. The key to utilize iterative optimization is to partition the problem into subproblems and solve each subproblem. Therefore, the computational complexity of the solution is reduced when compared to the case where the whole problem is solved without partitioning the problem. However, the problem we investigate do not possess such a property, therefore, we do not employ such an approach in this study.

III. Analysis

In this section, the results of numerical analysis are presented. MATLAB and general algebraic modeling system with CPLEX solver is used for the solutions of the MIP model presented in Section II.

We utilize two network topologies. The first one is the *square (grid)* topology, where the sensor nodes are located at the vertices of grid (internode distance is fixed to d_{int}) and the base station is at the center. The second topology is a *disk-shaped* network with the radius R_{net}, where the base station is located at the center of the disk and sensor nodes are deployed within the disk by using a random uniform distribution. For both topologies, we denote N_N as the number of nodes, which is taken as 81. Also for the transmission power levels on the links, we consider both the network level and link level approaches. In the first case, on each link, we utilize the maximum power level to reduce the packet errors (i.e., network level approach). For the second case, transmission power levels on each link is optimized through the local optimization scheme defined in (20) (i.e., link level approach). Since the path loss values are taking random values, we obtain our results with 100 different trials and average values are presented in each figure.

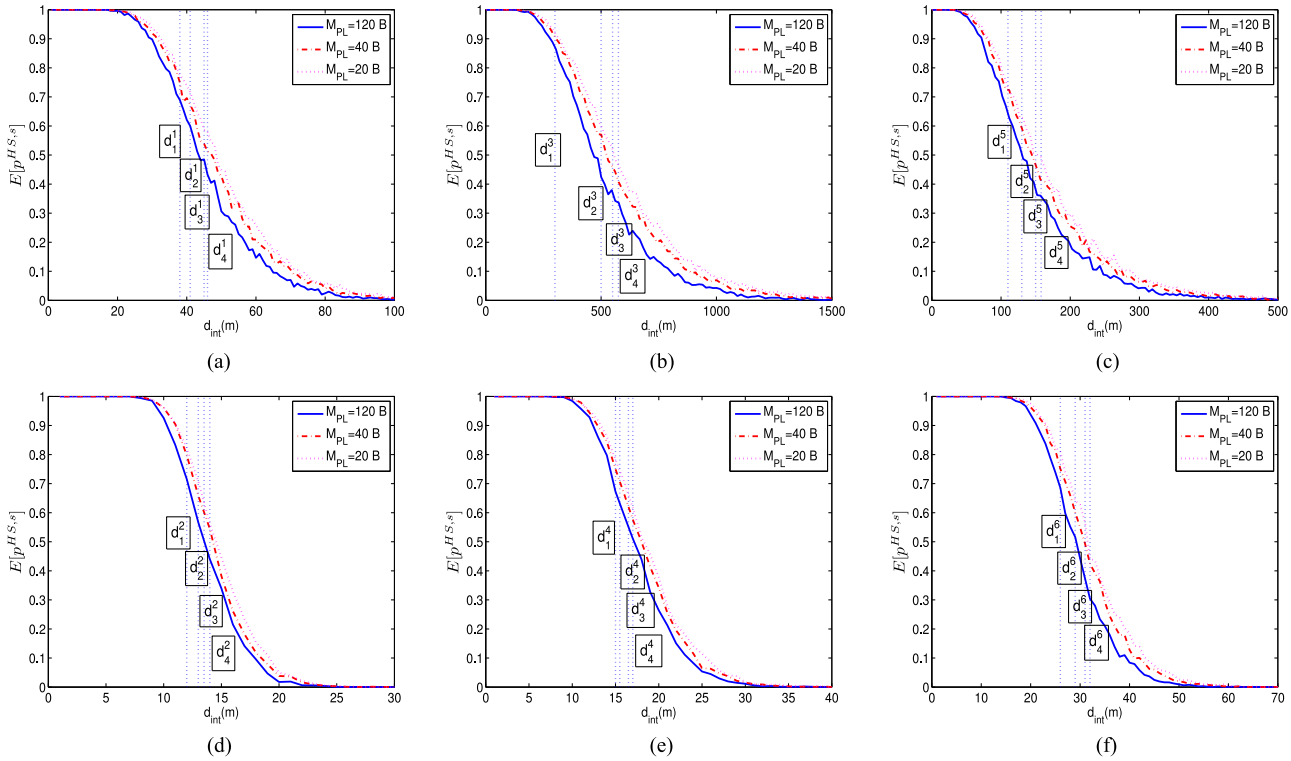

Fig. 2. Internode distance (d_{int}) versus avg. successful handshake probability ($E[p^{HS,s}]$) for the maximum power level ($l_{\text{max}} = 31$) deployed at the network level for six different SG environments with three different payload sizes (M_{PL}) (a) OUS-L, (b) UNT-L, (c) IMP-L, (d) OUS-N, (e) UNT-N, and (f) IMP-N.

In Fig. 2, we present the average successful handshake probability ($E[p^{HS,s}]$) with respect to (wrt.) the internode distance (d_{int}) for a two node pair (i.e., two nodes are separated by d_{int}). For this link, the maximum transmission power level ($l_{\text{max}} = 31$) is utilized and we consider the six different SG environments. In each subfigure, we present $E[p^{HS,s}]$ values for three different payload sizes (i.e., $M_{PL} = 120, 40$, and 20 Bytes). This figure is critical to understand the network lifetime optimization results present in the following figures.

In Table III, we mark d_{int} values which are denoted by d_n^m. The subscript n indicates the $E[p^{HS,s}]$ interval at that distance, while superscript m points the SG environment. We also present the corresponding optimum payload size (OPS) in Bytes and absolute lifetime (LT) in months at each d_n^m value. Note that, since successful handshake probabilities for different packet sizes are used, for a fixed d_n^m value, there exists a $E[p^{HS,s}]$ region rather than a fixed value. For different environments, $E[p^{HS,s}]$ regions are changing but roughly around 0.4–0.8. We obtain OPS values and LT values as follows: the MIP framework (given in Fig. 1) is solved for a 81-node grid topology and for the packet size value which yields the best lifetime (which is indeed the LT value) is considered as the OPS value. As the propagation environment becomes harsher (i.e., $E[p^{HS,s}]$ decreases), LT values decreases and the OPS values becomes smaller to maximize the network lifetime.

In Fig. 3, we show normalized lifetimes wrt. payload sizes for the six different SG environments when considering a square topology. For each curve we normalize the absolute lifetime values with the maximum lifetime value obtained at this configuration. In this figure, y-axis shows normalized lifetime values and x-axis denotes the payload sizes (M_{PL}) of 120, 60, 40, 30, 24, and 20 Bytes. We utilize the maximum transmission power level for all links. We observe that until a specific d_{int} value the network lifetime is maximum when the maximum packet size is utilized (i.e., when $M_{PL} = 120$ Bytes). As d_{int} increases, $E[p^{HS,s}]$ decreases and the maximum lifetime is obtained for smaller packet sizes. Nevertheless, this figure only includes d_{int} values, such that at least half of the 100 trials have connected networks (i.e., for larger d_{int}, more than half of the networks are disconnected, thus, the statistical reliability is compromised). From the point of view of SG environments, LOS or NLOS cases results in different lifetime results even for the same environment because path loss characteristics varies significantly for LOS and NLOS cases (presented in Table II).

We performed the same analysis as in Fig. 3 (not presented in the paper) by considering the local transmission power control scheme presented in (20). As we investigate the absolute lifetime values, transmission power level optimization increases the lifetime for this topology 0.72% on the average and 2.12% at maximum. If we compare the square networks with smaller d_{int} values, transmission power level optimization would provide better absolute lifetime values. Nevertheless, for the packet size optimization perspective, smaller d_{int} values yield the optimum packet size as the maximum one which does not help to answer the aforementioned questions given at the beginning of this section.

In Fig. 4, we present normalized lifetimes wrt. different payload sizes for a disk-shaped random topology with radius R_{net},

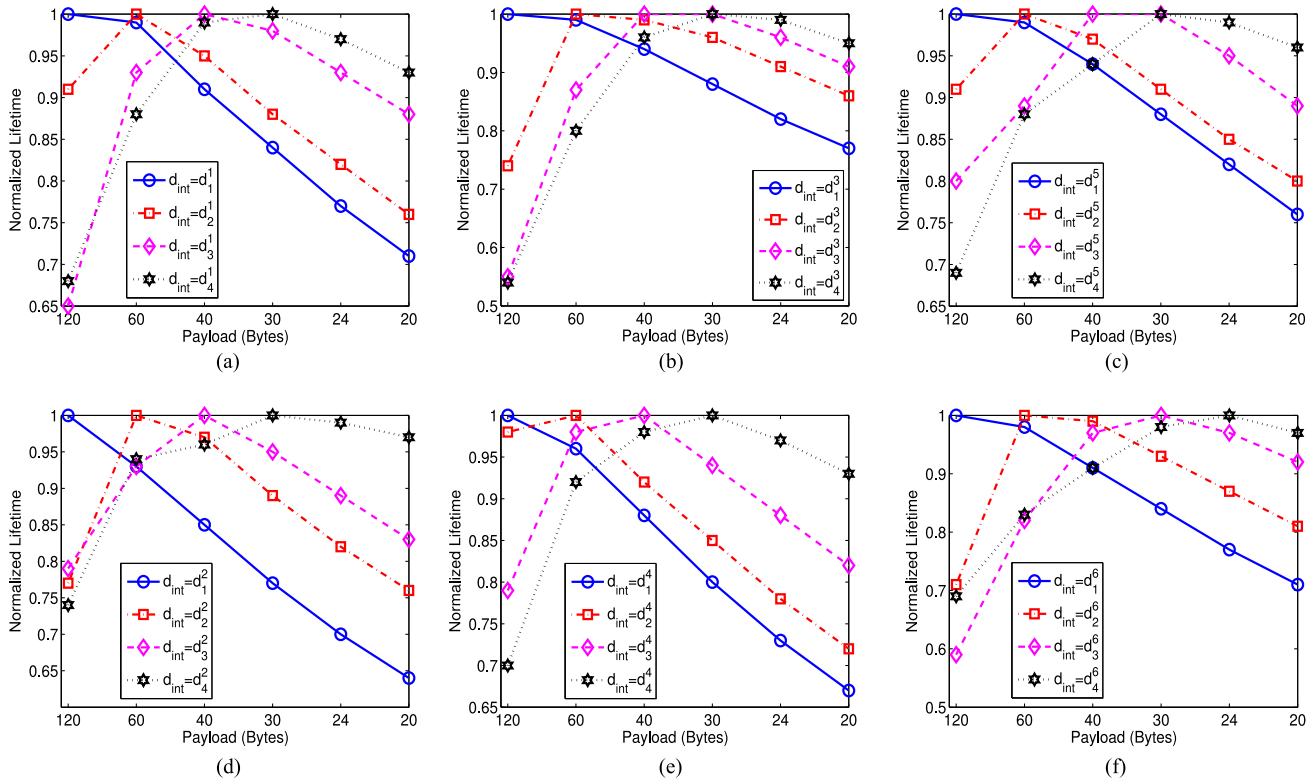

Fig. 3. Normalized lifetimes wrt. payload size for six different SG environments with max. power level ($l_{\max} = 31$) is deployed at the network level for various sized (wrt. to d_{int}) grid networks (a) OUS-L, (b) UNT-L, (c) IMP-L, (d) OUS-N, (e) UNT-N, and (f) IMP-N.

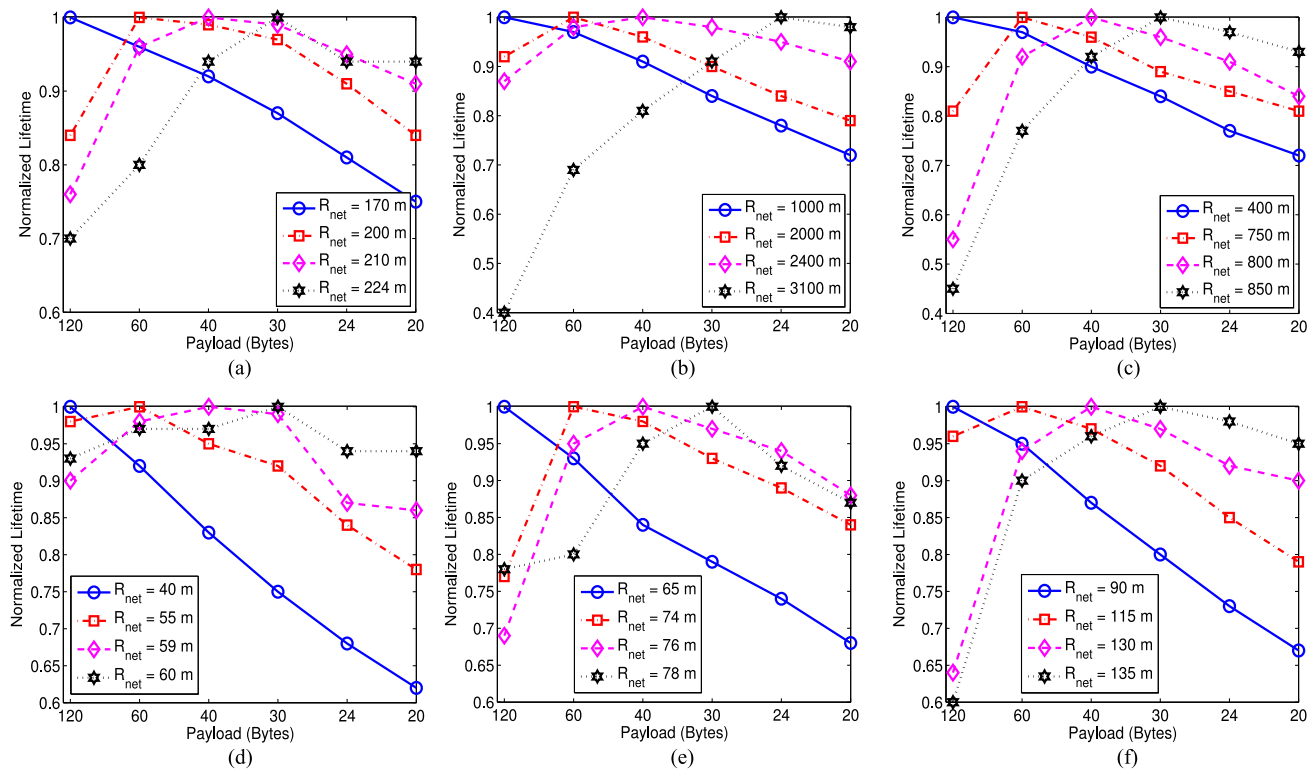

Fig. 4. Normalized lifetimes wrt. payload size for six different SG environments and power levels are optimized at the link level for various sized (wrt. to R_{net}) disk-shaped random networks (a) OUS-L, (b) UNT-L, (c) IMP-L, (d) OUS-N, (e) UNT-N, and (f) IMP-N.

TABLE III

MEASUREMENT POINTS ($d_{\text{INT}} = d_n^m$), CORRESPONDING AVG. SUCCESSFUL HANDSHAKE PROBABILITY INTERVALS ($E[p^{HS,s}]$), OPTIMUM PAYLOAD SIZES (OPS) IN BYTES, AND ABSOLUTE LIFETIME (LT) IN TERMS OF MONTHS (MO)

OUS-L					UNT-L					IMP-L				
d_{int}	Value	$E[p^{HS,s}]$	OPS (Bytes)	LT (mo)	d_{int}	Value	$E[p^{HS,s}]$	OPS (Bytes)	LT (mo)	d_{int}	Value	$E[p^{HS,s}]$	OPS (Bytes)	LT (mo)
d_1^1	38 m	0.7–0.8	120	20.5	d_1^3	300 m	0.85–0.9	120	57.0	d_1^5	110 m	0.65–0.75	120	33.2
d_2^1	41 m	0.6–0.75	60	15.5	d_2^3	500 m	0.45–0.6	60	14.8	d_2^5	130 m	0.55–0.65	60	20.9
d_3^1	45 m	0.5–0.6	40	9.5	d_3^3	550 m	0.4–0.55	40	10.3	d_3^5	150 m	0.4–0.5	40	12.3
d_4^1	46 m	0.45–0.6	30	8.0	d_4^3	575 m	0.35–0.5	30	8.5	d_4^5	158 m	0.35–0.5	30	9.7
OUS-N					UNT-N					IMP-N				
d_{int}	Value	$E[p^{HS,s}]$	OPS (Bytes)	LT (mo)	d_{int}	Value	$E[p^{HS,s}]$	OPS (Bytes)	LT (mo)	d_{int}	Value	$E[p^{HS,s}]$	OPS (Bytes)	LT (mo)
d_1^2	12 m	0.7–0.8	120	17.6	d_1^4	15 m	0.65–0.8	120	17.6	d_1^6	26 m	0.7–0.8	120	17.0
d_2^2	13 m	0.6–0.75	60	11.4	d_2^4	15.5 m	0.65–0.75	60	15.0	d_2^6	29 m	0.55–0.65	60	10.6
d_3^2	13.5 m	0.5–0.6	40	9.6	d_3^4	16.5 m	0.55–0.7	40	10.5	d_3^6	31 m	0.4–0.55	30	7.1
d_4^2	14 m	0.45–0.6	30	6.3	d_4^4	17 m	0.5–0.65	30	7.6	d_4^6	32 m	0.35–0.5	24	5.3

where nodes are uniformly distributed within the disk. We assume that all links are utilizing the optimum power transmission level (according to (20)). R_{net} is changed for each SG environment to investigate the effects of packet size on the network lifetime. For smaller R_{net} values, largest packets yield the best network lifetime, while when we increase R_{net}, smaller packet sizes are favored to obtain the maximum network lifetime. Comparing previous plots, it should be noted that lifetime characteristics differ from that of the square grid topology.

We investigated the $p^{HS,s}$ distribution of the utilized links. As a general trend, majority of the data flows are on links with $p^{HS,s} \geq 0.98$ (e.g., more than half of the data, flow over all links with $p^{HS,s} \geq 1.00$). Another noteworthy observation on the characteristics of the $p^{HS,s}$ values of the utilized links is that $0.6 \leq p^{HS,s} \leq 0.7$ band is also utilized more than the other $p^{HS,s}$ values. These links are the ones where the retransmissions occurred frequently. In this region, the optimization framework provides alternative ways with smaller number of hops to reduce the energy dissipation than the case of multihops for larger $p^{HS,s}$. Furthermore, the percentage of use for very high $p^{HS,s}$ valued links with 0.98–0.99 are smaller for sparser networks.

Till this point, we assume that no *sensitivity threshold* is applied in sensor nodes. If the usage of a link is prohibited when the received power is lesser than a sensitivity threshold, then how does the network lifetime get affected? This question can be answered by adding a condition to (4) and (5); a link usage is allowed if and only if received antenna powers both at data and ACK receiving nodes are greater than the sensitivity threshold which can be mathematically expressed as $P_{rx,ij}^{\text{ant}}(l) \geq P_{\text{sns}}$ and $P_{rx,ji}^{\text{ant}}(k) \geq P_{\text{sns}}$. In this notation, P_{sns} denotes the nominal receiver sensitivity.

To analyze the effects of the *sensitivity threshold*, we use the same disk-shaped random topology as in Fig. 4. However, we only use the second R_{net} values (e.g., $R_{\text{net}} = 200$ m for OUS-L, $R_{\text{net}} = 2000$ m for UNT-L, etc.) presented in Fig. 4. P_{sns} values are given as -100, -97, -94, -90 dBm, where the last two ones are typical and maximum threshold values for Tmote Sky motes, respectively [30] (we do not present the figure in the paper, however, we present the main results of the analysis). For most of the environments, setting a P_{sns} threshold value changes the optimum packet size value that yields the maximum lifetime. Furthermore, setting higher threshold values (e.g., $P_{\text{sns}} = -90$ dBm) results in disconnected networks even if they are connected in the case where P_{sns} threshold is inactive.

In our evaluations, we utilized highly stable propagation environments, therefore, path loss values do not vary within each scenario. Nevertheless, we presented the averages of 100 randomly generated scenarios and path loss values of the links in each scenario exhibit significant variations. Hence, as long as fairly accurate path loss estimation capability is available, our conclusions are not affected by the channel condition variations. In fact, channel condition monitoring in WSNs can be done with very low overhead and with high accuracy as shown in [41] through direct experimentation.

Since our MIP problem is an NP-complete problem its computational complexity is high. Furthermore, as the number of nodes increase, the computational complexity increases rapidly. Therefore, efficient heuristics are necessary for the efficient solution of the optimization problem. As an alternative to the exact solution of the MIP problem, we solve the optimization problem by linear programming (LP) relaxation, where integer variables of the original MIP problem are treated as continuous variables. Note that LP problems can be solved in polynomial time, however, the LP-relaxed solutions do not necessarily result in integral solutions (e.g., 1245.2 packets flowing on a particular link). Nevertheless, the target in LP-relaxation is to closely approximate the optimal solution with low computational complexity. For all the problems we present, in this paper, we obtained the exact integer solutions and LP-relaxation solutions. The maximum difference between the exact and LP-relaxed solutions is upper bounded by 0.001%. To illustrate the performance of the LP-relaxation solution in comparison to the exact solution through an example, we present the $R_{\text{net}} = 170$ m solutions of Fig. 4(a) in Table IV. The maximum difference between the exact and LP-relaxation solutions are upper limited by 0.00021%. Furthermore, the solution times of LP-relaxation solutions are significantly lower than the solution times of the exact integer solutions.

The most important factor affecting the computation time is the number of nodes in the network. To determine the effects of N_N, we present the comparative performance results and solution times for the exact and LP-relaxed solutions in Table V.

TABLE IV
LIFETIME DIFFERENCE (%) BETWEEN LP-RELAXATION AND EXACT SOLUTIONS WITH AVERAGE SOLUTION TIMES AS A FUNCTION OF PAYLOAD SIZE FOR OUS-L ENVIRONMENT WHERE THE POWER LEVELS ARE OPTIMIZED AT LINK LEVEL WHEN $R_{\text{net}} = 170$ M AND $N_N = 81$ FOR DISK-SHAPED RANDOM NETWORKS

		Avg. Solution Time (s)	
Payload (Bytes)	Lifetime Difference (%)	LP Relaxation	Exact
120	0.00009	3.31	22.12
60	0.00018	3.22	19.51
40	0.00019	3.21	18.18
30	0.00020	3.21	16.63
24	0.00021	3.23	14.57

TABLE V
MAXIMUM LIFETIME DIFFERENCE (%) BETWEEN LP-RELAXATION AND EXACT SOLUTION WITH AVERAGE SOLUTION TIMES AS A FUNCTION OF N_N FOR OUS-L ENVIRONMENT WHERE THE POWER LEVELS ARE OPTIMIZED AT LINK LEVEL WHEN $R_{\text{net}} = 170$ M FOR DISK-SHAPED RANDOM NETWORKS ($M_{PL} = 24$ BYTES)

		Avg. Solution Time (s)	
N_N	Max. Lifetime Difference (%)	LP Relaxation	Exact
121	0.00010	8.19	45.03
101	0.00018	5.44	34.46
81	0.00021	3.23	14.57
61	0.00027	1.82	2.01
41	0.00032	0.87	0.92

Indeed, solution times increase as N_N increases for both the exact solution and the LP-relaxation solution, however, the solution times obtained for the exact solution increase with a much higher pace than the LP-relaxed solution as N_N increases.

IV. CONCLUSION

In this study, we proposed a realistic WSN link layer energy dissipation model for Tmote Sky platforms and an MIP framework to jointly optimize the transmission power level and data packet size. We gave a special attention not only to the harsh conditions of the SG environments (e.g., high path loss, low SNR, and high BER values), but also the practical aspects, such as packet retransmission mechanism, changing the packet size according to the channel conditions, and enforcing a sensitivity threshold. Our main conclusions are itemized as follows.

1) Considering an SG environment with high $p^{HS,s}$ links, the optimum packet size is the *largest* packet size that is available, however, for a harsh SG environment (*i.e.*, low $p^{HS,s}$ valued links), the optimum packet size decreases to attain maximum lifetime.
2) Although transmission power control increases the absolute lifetime, normalized network lifetime does not vary significantly as a function of packet size, therefore, due to the dominance of the propagation environment, transmission power optimization is not the sole mechanism in determining the optimum packet size.
3) In denser networks, most of the data flow on the links with very high $p^{HS,s}$ values so the highest possible packet size is utilized, however, for sparse networks, high $p^{HS,s}$ valued links are scarcer and smaller packet sizes are utilized for maximizing the WSN lifetime.
4) Elimination of the utilization of certain links with received power below a predetermined threshold (i.e., the sensitivity threshold) can change the packet size that is optimum for network lifetime. For a given network configuration, for higher sensitivity thresholds, larger packet sizes are favored.
5) The optimum design decisions for WSNs employed in SG environments with the objective of lifetime maximization are to deploy sensor nodes in such a fashion that communication links do not have path loss values that force the transceivers to operate deep in the transitional region, utilize the highest packet size possible, and assign optimal transmission power levels for both data and ACK packets.

Validation of the link layer, energy dissipation model, and results of our analysis through experimental evaluations in WSN testbeds, and extending the proposed framework utilizing different physical layer models and network topologies are important future research directions.

REFERENCES

[1] J. Varela *et al.*, "Show me!: Large-scale smart grid demonstrations for European distribution networks," *IEEE Power Energy Mag.*, vol. 13, no. 1, pp. 84–91, Jan./Feb. 2015.
[2] J. Lee, J. Guo, J. K. Choi, and M. Zukerman, "Distributed energy trading in microgrids: A game-theoretic model and its equilibrium analysis," *IEEE Trans. Ind. Electron.*, vol. 62, no. 6, pp. 3524–3533, Jun. 2015.
[3] V. C. Gungor, L. Bin, and G. P. Hancke, "Opportunities and challenges of wireless sensor networks in smart grid," *IEEE Trans. Ind. Electron.*, vol. 57, no. 10, pp. 3557–3564, Oct. 2010.
[4] E. Fadel *et al.*, "A survey on wireless sensor networks for smart grid," *Comput. Commun.*, vol. 71, pp. 22–33, Nov. 2015.
[5] J. Han, J. Hu, Y. Yang, Z. Wang, S. X. Wang, and J. He, "A nonintrusive power supply design for self-powered sensor networks in the smart grid by scavenging energy from ac power line," *IEEE Trans. Ind. Electron.*, vol. 62, no. 7, pp. 4398–4407, Jul.2015.
[6] M. Chen, "Reconfiguration of sustainable thermoelectric generation using wireless sensor network," *IEEE Trans. Ind. Electron.*, vol. 61, no. 6, pp. 2776–2783, Jul.2014.
[7] M. Li and H. J. Lin, "Design and implementation of smart home control systems based on wireless sensor networks and power line communications," *IEEE Trans. Ind. Electron.*, vol. 62, no. 7, pp. 4430–4442, Jul.2015.
[8] M. Yigit, E. A. Yoney, and V. C. Gungor, "Performance of MAC protocols for wireless sensor networks in harsh smart grid environment," in *Proc. IEEE Int. Black Sea Conf. Commun. Netw.*, 2013, pp. 50–53.
[9] H. U. Yildiz, S. Kurt, and B. Tavli, "The impact of near-ground path loss modeling on wireless sensor network lifetime," in *Proc. IEEE Mil. Commun. Conf.*, 2014, pp. 1114–1119.
[10] H. U. Yildiz, B. Tavli, and H. Yanikomeroglu, "Transmission power control for link-level handshaking in wireless sensor networks," *IEEE Sensors J.*, vol. 16, no. 2, pp. 561–576, Jan. 2016.
[11] B. E. Bilgin and V. C. Gungor, "On the performance of multi-channel wireless sensor networks in smart grid environments," in *Proc. Int. Conf. Comput. Commun. Netw.*, 2011, pp. 1–6.
[12] M. Leghari, S. Abbasi, and L. D. Dhomeja, "Survey on packet size optimization techniques in wireless sensor networks," in *Proc. Int. Conf. Wireless Sensor Netw.*, 2013, pp. 1–8.
[13] Y. Sankarasubramaniam, I. F. Akyildiz, and S. W. McLaughlin, "Energy efficiency based packet size optimization in wireless sensor networks," in *Proc. IEEE Int. Workshop Sensor Netw. Protocols Appl.*, 2003, pp. 1–8.

[14] W. Dong *et al.*, "DPLC: Dynamic packet length control in wireless sensor networks," in *Proc. IEEE Conf. Comput. Commun.*, 2010, pp. 1–9.
[15] M. Holland, T. Wang, B. Tavli, A. Seyedi, and W. Heinzelman, "Optimizing physical-layer parameters for wireless sensor networks," *ACM Trans. Sensor Netw.*, vol. 7, no. 4, pp. 28–1-28-20, Feb. 2011.
[16] M. C. Oto and O. B. Akan, "Energy-efficient packet size optimization for cognitive radio sensor networks," *IEEE Trans. Wireless Commun.*, vol. 11, no. 4, pp. 1544–1553, Apr. 2012.
[17] Y. Li *et al.*, "Communication energy modeling and optimization through joint packet size analysis of BSN and WiFi networks," *IEEE Trans. Parallel Distrib. Syst.*, vol. 24, no. 9, pp. 1741–1751, Sep. 2013.
[18] C. Noda, S. Prabh, M. Alves, and T. Voigt, "On packet size and error correction optimisations in low-power wireless networks," in *Proc. IEEE Conf. Sensor Mesh Ad Hoc Commun. Netw.*, 2013, pp. 212–220.
[19] A. Akbas, H. U. Yildiz, and B. Tavli, "Data packet length optimization for wireless sensor network lifetime maximization," in *Proc. Int. Conf. Commun.*, 2014, pp. 1–6.
[20] J. S. Karthi, S. V. Rao, and S. S. Pillai, "Impact of IEEE 802.11 MAC packet size on performance of wireless sensor networks," *IOSR J. Electron. Commun. Eng.*, vol. 10, no. 3, pp. 6–11, May/Jun. 2015.
[21] S. Basagni, C. Petrioli, R. Petroccia, and M. Stojanovic, "Optimized packet size selection in underwater wireless sensor network communications," *IEEE J. Ocean. Eng.*, vol. 37, no. 3, pp. 321–337, Jul.2012.
[22] M. Ayaz, L. T. Jung, A. Abdullah, and I. Ahmad, "Reliable data deliveries using packet optimization in multi-hop underwater sensor networks," *J. King Saud Univ. Comput. Inf. Sci.*, vol. 24, no. 1, pp. 41–48, Jan. 2012.
[23] M. Stojanovic, "Optimization of a data link protocol for an underwater acoustic channel," in *Proc. IEEE Eur. Oceans*, 2005, vol. 1, pp. 68–73.
[24] L. T. Jung and A. B. Abdullah, "Underwater wireless network energy efficiency and optimal data packet size," in *Proc. Int. Conf. Elect. Control Comput. Eng.*, 2011, pp. 178–182.
[25] M. Vuran and I. F. Akyildiz, "Cross-layer packet size optimization for wireless terrestrial, underwater, and underground sensor networks," in *Proc. IEEE Conf. Comput. Commun.*, 2008, pp. 780–788.
[26] N. Yaakob and I. Khalil, "Packet size optimization for congestion control in pervasive healthcare monitoring," in *Proc. IEEE Int. Conf. Inf. Technol. Appl. Biomed.*, 2010, pp. 1–4.
[27] M. C. Domingo, "Packet size optimization for improving the energy efficiency in body sensor networks," *ETRI J.*, vol. 33, no. 3, pp. 299–309, Jun. 2011.
[28] M. S. Mohammadi, Q. Zhang, E. Dutkiewicz, and X. Huang, "Optimal frame length to maximize energy efficiency in IEEE 802.15.6 UWB body area networks," *IEEE Wireless Commun. Lett.*, vol. 3, no. 4, pp. 397–400, Aug. 2014.
[29] N. Kilic and V. C. Gungor, "Analysis of low power wireless links in smart grid environments," *Comput. Netw.*, vol. 57, no. 5, pp. 1192–1203, Apr. 2013.
[30] *Tmote Sky datasheet*. (2006). [Online]. Available: http://www.eecs.harvard.edu/ konrad/projects/shimmer/references/tmote-sky-datasheet.pdf
[31] K. Bicakci, H. Gultekin, and B. Tavli, "The impact of one-time energy costs on network lifetime in wireless sensor networks," *IEEE Commun. Lett.*, vol. 13, no. 12, pp. 905–907, Dec. 2009.
[32] H. Cotuk, B. Tavli, K. Bicakci, and M. B. Akgun, "The impact of bandwidth constraints on the energy consumption of wireless sensor networks," in *Proc. IEEE Wireless Commun. Netw. Conf.*, 2014, pp. 2787–2792.
[33] G. Lu, B. Krishnamachari, and C. S. Raghavendra, "An adaptive energy-efficient and low-latency MAC for data gathering in wireless sensor networks," in *Proc. Int. Parallel Distrib. Process. Symp.*, 2004, pp. 224–231.
[34] G. Anastasi, M. Conti, A. Falchi, E. Gregori, and A. Passarella, "Performance measurements of motes sensor networks," in *Proc. ACM Int. Conf. Model. Anal. Simul. Wireless Mobile Syst.*, 2004, pp. 174–181.
[35] M. Schuts, F. Zhu, F. Heidarian, and F. W. Vaandrager, "Modelling clock synchronization in the chess gMAC WSN protocol," in *Proc. 1st Workshop Quant. Formal Methods Theory Appl.*, 2009, vol. 13, pp. 41–54.
[36] S. Kurt and B. Tavli, "Propagation model alternatives for outdoor wireless sensor networks," in *Proc. IFIP Wireless Days*, 2013, pp. 1–3.
[37] T. Rappaport, *Wireless Communications: Principles and Practice*, 2nd ed. Englewood Cliffs, NJ, USA: Prentice-Hall, 2001.
[38] S. Lanzisera and K. Pister, "Theoretical and practical limits to sensitivity in IEEE 802.15.4 receivers," in *Proc. IEEE Int. Conf. Electron. Circuits Syst.*, 2007, pp. 1344–1347.
[39] H. Cotuk, K. Bicakci, B. Tavli, and E. Uzun, "The impact of transmission power control strategies on lifetime of wireless sensor networks," *IEEE Trans. Comput.*, vol. 63, no. 11, pp. 2866–2879, Nov. 2014.
[40] Z. Nutov and M. Segal, "Improved approximation algorithms for maximum lifetime problems in wireless networks," *Theor. Comput. Sci.*, vol. 453, pp. 88–97, Sep. 2012.
[41] S. Linetal., "ATPC: Adaptive transmission power control for wireless sensor networks," *ACM Trans. Sensor Netw.*, vol. 12, no. 1, pp. 6–1–6-31, Mar. 2016.

Sinan Kurt received the B.S. and M.S. degrees from the Middle East Technical University, Ankara, Turkey, in 2004 and 2007, respectively, and the Ph.D. degree from the TOBB University of Economics and Technology, Ankara, in 2016, all in electrical and electronics engineering.

He is a Lead Design Engineer at ASELSAN Inc., Ankara. His research interests include the areas of wireless communications, electromagnetics, circuit design, wireless networks, and optimization.

Huseyin Ugur Yildiz (S'13–M'16) received the B.S. degree from Bilkent University, Ankara, Turkey, in 2009, and the M.S. and Ph.D. degrees from TOBB University of Economics and Technology, Ankara, Turkey, in 2013 and 2016, respectively, all in electrical and electronics engineering.

He is currently an Assistant Professor in the Department of Electrical and Electronics Engineering, TED University, Ankara, Turkey. His research focuses on the applications of optimization techniques to modeling and analyzing research problems on wireless communications and networks.

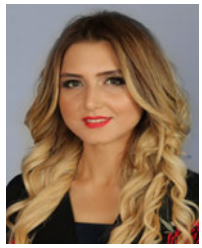

Melike Yigit received the B.S. and M.S. degrees in computer engineering in 2010 and 2012, respectively, from Bahcesehir University, Istanbul, Turkey, where she is currently working toward the Ph.D. degree.

She is also currently working at Turkish Airlines (THY) as a Business Analyst.

Bulent Tavli (S'97–M'05) received the B.S. degree in electrical and electronics engineering from the Middle East Technical University, Ankara, Turkey, in 1996, and the M.S. and Ph.D. degrees in electrical and computer engineering from the University of Rochester, Rochester, NY, USA, in 2002 and 2005, respectively.

He is a Professor in the Electrical and Electronics Engineering Department, TOBB University of Economics and Technology, Ankara. His current research interests include wireless communications, networking, optimization, embedded systems, information security, and smart grid.

Vehbi Cagri Gungor received the B.S. and M.S. degrees in electrical and electronics engineering from the Middle East Technical University, Ankara, Turkey, in 2001 and 2003, respectively, and the Ph.D. degree in electrical and computer engineering from the Georgia Institute of Technology, Atlanta, GA, USA, in 2007.

He is currently an Associate Professor and the Chair of the Computer Engineering Department, Abdullah Gul University, Kayseri, Turkey.